Electrochimica Acta 157 (2015) 299–306

Contents lists available at ScienceDirect

Electrochimica Acta

journal homepage: www.elsevier.com/locate/electacta

Increasing the reversibility of Li–O_2 batteries with caterpillar structured α–MnO_2/N–GNF bifunctional electrocatalysts

Awan Zahoor [a], Maria Christy [b], Hosaeng Jang [a], Kee Suk Nahm [a,b,*], Yun Sung Lee [c,**]

[a] School of Chemical Engineering and R&D Education Centre for Fuel Cell Materials & Systems, Chonbuk National University, Jeonju 561-756, Republic of Korea
[b] R&D Education Centre for Fuel Cell Materials & Systems, Chonbuk National University, Jeonju, 561-756, Republic of Korea
[c] Faculty of Applied Chemical Engineering, Chonnam National University, Gwangju 500-757, Republic of Korea

ARTICLE INFO

Article history:
Received 22 September 2014
Received in revised form 27 December 2014
Accepted 13 January 2015
Available online 14 January 2015

Keywords:
Li–O_2 battery
Bifunctional electrocatalyst
Nitrogen doping
Hybrid material
α–MnO_2

ABSTRACT

The high performance of α–MnO_2/NGNF catalyzed air cathode for Li–O_2 battery is reported in this article. The α–MnO_2 nanorods are successfully grown on highly conductive nitrogen doped graphite nanofibers with caterpillar like morphology by a simple hydrothermal technique. The as–prepared α–MnO_2/N–GNF catalyst exhibits better electrocatalytic performance in terms of oxygen reduction and evolution reactions in the air cathode exhibiting comparatively low overpotential. In addition to the low overpotential, α–MnO_2/NGNF catalyzed Li–O_2 battery also show high capacity, reversibility and rate capability. The combined effect of α–MnO_2 and N–GNF for facilitating electrochemical reactions between Li and O_2 is described for improving energy and columbic efficiency of Li–O_2 battery.

1. Introduction

Li–air battery has taken a massive leap forward with increased number of research publications in the past few years. This attention is mainly because of its exceptionally higher gravimetric energy storage density comparable to that of gasoline [1,2]. Yet there are various aspects to be considered to make this technology practically possible. The overall electrochemical reaction of the battery can be expressed as $2(Li^+ + e^-) + O_2 \Leftrightarrow Li_2O_2$; during which oxygen reduction reaction (ORR) takes place on discharge process (forward), followed by the oxygen evolution reaction (OER) on charging (reverse). One of the major problems in Li–air batteries is the formation of undesired discharge products besides Li_2O_2. In many cases the discharge product from oxygen reduction reaction (ORR) on cathode is not only Li_2O_2. There are other products which are also formed that can easily react with the electrolytes to form organic lithium salt degrading the cell cyclability rapidly. Another major problem which hurdles this technology is the very large potential difference between the ORR and OER in cathode resulting in low round trip efficiency [3]. The former problem is being investigated with various suitable electrolytes, while it is hoped that the development of better electrocatalysts can solve the latter by reducing the overpotential and increasing the cyclability of the battery [4,5].

Catalysts are one of the most important materials that influence the charge/discharge process in Li–air batteries. The ORR and OER at the air–cathode of Li–O_2 batteries are important processes which control the overall cell performance [5]. Hence it is necessary to develop efficient ORR and OER bi-functional electrocatalyst. Precious metal catalysts such as Au, Pd, Pt etc., [6–8] and metal oxide catalysts like Fe_2O_3, Co_3O_4 and MnO_2 [9,10] have been investigated as potential catalyst materials that control the performance of oxygen electrodes. Particularly, after the significantly high capacity with α–MnO_2 nanowires catalyst was reported by Debart et al. in 2008 [10], there have been vigorous investigations on α–MnO_2 nanomaterials to optimize the performance. Recently Kang et al. [11] also reported a high capacity Li–O_2 battery with α–MnO_2 nanowires as catalysts with a stable cyclability for 20 cycles with limited depth of discharge. In our previous report, we have reported the high electrocatalytic activity of 3 dimensional α–MnO_2 nanourchins on air cathode. The α–MnO_2 catalyzed electrodes exhibited a stable cycling performance with increased discharge capacity and reduced overpotential [12]. Hu et al. [13] also reported the application of porous manganese oxide nanostructures in Li-O_2 batteries. Even though α–MnO_2 with different structures and morphologies have

* Corresponding author. Tel.: +82 63 270 2311; fax: +82 63 270 3909.
** Corresponding author. Tel.: +82 62 530 1904.
E-mail addresses: nahmks@jbnu.ac.kr (K.S. Nahm), leeys@chonnam.ac.kr (Y.S. Lee).

http://dx.doi.org/10.1016/j.electacta.2015.01.058
0013-4686/

been synthesized and applied as suitable catalysts in Li–O_2 batteries, the catalytic activity is still far below the commercial Pt based catalysts.

The reason for the underperformance could be the low electrical conductivity of manganese oxide nanomaterials. In order to improve the electrocatalytic activity, one of the desirable methods is to combine or grow the α–MnO_2 catalysts on a highly conductive support. Guan et al. [14] optimized the α–MnO_2 catalysts by coating them directly on multi-walled carbon nanotubes. They observed enhanced oxygen reduction and evolution reactions, and improved energy efficiency and cyclability. Yu et al. and others [15–17] have assured that rGO/α–MnO_2 composite can potentially make a good cathode for Li–air batteries and other energy storage devices. They have identified the roles of reduced graphene oxide and other graphene based materials in sustaining relatively high capacities with α–MnO_2 composite electrodes. Chen et al., [18] introduced nitrogen–doped exfoliated graphene and α–MnO_2 nanotube composite as ORR active air cathode material for Li–O_2 battery applications. They observed improved ORR activity of the material due to the addition of superior electronic property of graphene and the defective sites generated by nitrogen doping. Graphite nanofibers (GNF) with its unique properties like high conductivity and decreased impurities are suitable catalyst support which has been investigated intensively for various applications [19–21]. Owing to the large surface area, flexibility, and chemical stability, graphite has always been an excellent substrate to host active nanomaterials. Also, preferred crystallographic orientation of α–MnO_2 can be attained as a result of interaction in the highly ordered GNF substrate [19–21]. But GNF has not yet been utilized as catalyst support for Li–O_2 battery applications to the best of our knowledge even though CNF electrodes can provide gravimetric energies up to 2500 $Whkg^{-1}$ at powers up to 100 Wkg^{-1}, which are among the highest values reported for Li–O_2 batteries to date (including carbon-only and catalyst-containing electrodes) [22].

In this work, we have grown α–MnO_2 nanorods on highly conductive graphite nanofibers (GNF) with caterpillar like morphology for electrocatalytic application. In addition we doped the GNF with nitrogen (N) (here after called as N–GNF) before growing α–MnO_2, because it is well established that incorporation of nitrogen increases the activity by introducing structural defects [23,24]. The as-prepared α–MnO_2/N–GNF nanomaterials were examined for ORR and OER activities in the air cathode of Li–O_2 cell. The α–MnO_2 nanorods grown on N–GNF exhibited high capacity and reversibility with low overpotential. The better performance of Li–O_2 battery with caterpillar shaped α–MnO_2/N–GNF obtained in our experiment is far better than other previous reports [10,15,23].

2. Experimental method

GNF materials were commercially purchased from (Carbon nanomaterial technology, co., Ltd) and doped with nitrogen. We employed the nitrogen doping process that was utilized in our previous report [24] with negligible modification. The α–MnO_2 nanorods were then grown on N–GNF by simple hydrothermal technique [12] based on our mechanistic study on phase and morphology conversion of MnO_2 nanostructures [26]. $KMnO_4$ was mixed with N–GNF under mortar and pestle condition and dispersed the mixture into 30 ml DI water. Later 250 μl H_2SO_4 was added into the solution. Finally hydrothermal treatment was performed at 80 °C for one hour. The as-prepared sample was wash with DI water and dried under vacuum. Thus obtained final product was α–MnO_2/N–GNF nanostructure.

The as–prepared material was characterized by x–ray diffraction spectrum (XRD, X'PERT–MRD, Philips) to identify the phase and crystal structure. The morphology of the prepared composite was analyzed by field emission scanning electron microscopy (FESEM) (S–4700, HITACHI) and transmission electron microscopy (TEM). X–ray photoelectron spectroscopy (XPS) analysis was performed using a thermo scientific Kα x–ray source, which was used to confirm the nitrogen doping in GNF. EDX analysis was utilized to identify the chemical composition of the grown nanostructure. Brunauer–Emmett–Teller (BET) (BEL SORP Bell Japan Inc.) surface area analysis was employed to study the specific surface properties of the synthesized nanocomposite.

For lithium battery studies, the α–MnO_2/N–GNF catalyst and conductive KB carbon were mixed in the ratio of 1:2 with teflonised acetelyn black binder in iso–propyl alcohol and made into a pellet type electrode. The pellet was pressed on Ni mesh current collector, dried over night at 100 °C and employed as cathode. The performance of α–MnO_2/N–GNF catalyst for ORR/OER in Li–O_2 air cathode was evaluated in a Swagelok™ type cells with 1 M LiTFSI (TEGDME) electrolyte and Li anode. The Li–O_2 cell performance was tested galvanostatically in a potential window of 2∼4.3 V in a BTS 2004 (JAPAN) battery tester at different current densities (0.1, 0.2 and 0.3 mA/cm^2) in room temperature and 1 atm O_2 atmosphere.

3. Results and Discussion

3.1. Physical properties

Shown in Fig. 1 are the XRD spectra for α–MnO_2, GNF, N–GNF and α–MnO_2/N–GNF, respectively. The synthesized MnO_2 material shows characteristic α–MnO_2 XRD peaks at 2θ (110), (200), (310), (211), (301), (411), (600), (521) and (002), which coincide with JCPDS 44-0141, and GNF material exhibits characteristic carbon peaks around 2θ = 26° corresponding to (002) graphitic planes, as shown in Fig. 1. The α–MnO_2/NGNF shows both the α–MnO_2 and graphite related peaks, which identify the growth of α–MnO_2 over N–GNF. To confirm the doping of nitrogen in N–GNF, XPS spectrum was obtained. The XPS spectrum in Fig. 2(a) shows the presence of N and O in N–doped GNF (N–GNF) by identifying N1s and O1s at binding energies of 397.7 and 533 eV, respectively [25]. EDX elemental analysis clearly given in Fig. 2(b) shows that the surface of α–MnO_2/N–GNF structures are mainly

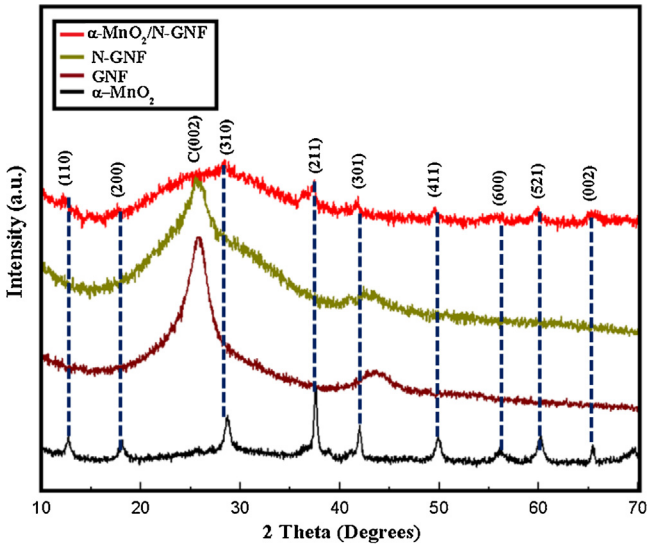

Fig. 1. X–ray diffraction of spectra of α-MnO_2, GNF, N–GNF and α–MnO_2/NGNF nanomaterials.

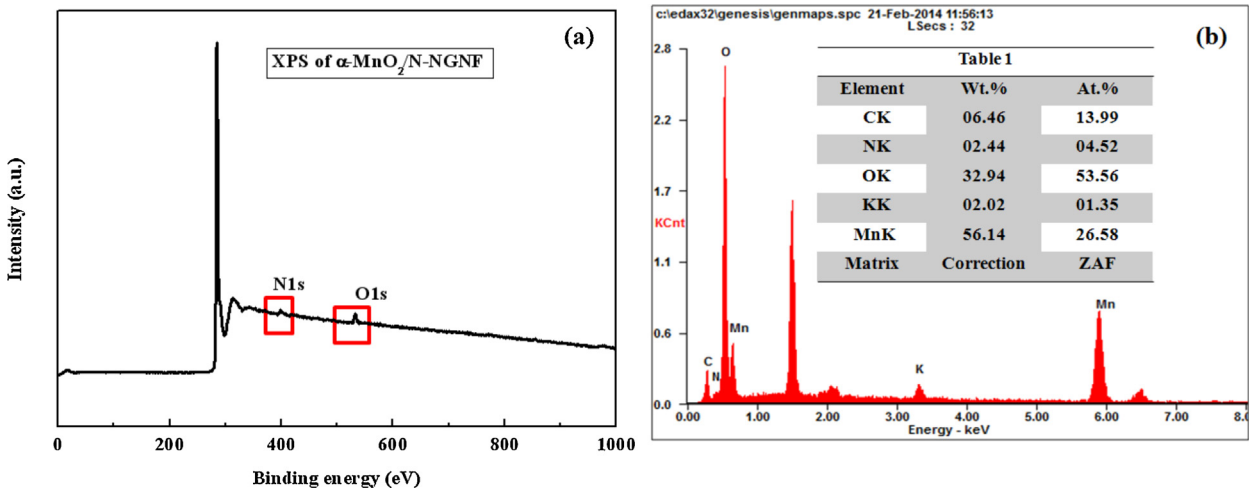

Fig. 2. (a) XPS spectrum of N–GNF and (b) EDX spectrum of α–MnO_2/NGNF. (Inset Table 1 shows EDX elemental analysis).

composed of MnO_2 (inset Table 1 in Fig. 2(b)), indicating the growth of α–MnO_2 structures on N–doped GNF.

The morphological characteristics of the synthesized α–MnO_2/N–GNF material are given in Fig. 3. The as-purchased graphite nanofibers in Fig 3(a) show rich fibrous structures of 130–170 nm diameters with some organic and carbon residues. After N doping, however, the residues are completely removed and the smoothly surfaced N–GNF structure appears as shown in Fig 3(b). During the N–doping process, it is considered that NH_3 gas is decomposed into highly active chemical radicals, which could react with the residues to leave the smooth surface [24,25]. From Fig 3(c), it is seen that α–MnO_2 structures consisting of small nanorods are grown all over N–GNF nanostructures with caterpillar like structures. The TEM images given in Fig. 3(d) also show the formation of α–MnO_2 consisting of small nanorods grown on N–GNF. The HRTEM of the nanorod has a lattice distance of 0.52 nm, which corresponds to the (2 0 0) plane of α–MnO_2 [26]. This value corresponds to the characteristic (2 0 0) plane of α–MnO_2 as observed in XRD pattern.

The surface properties of synthesized α–MnO_2/N–GNF nanomaterials were investigated with BET analysis. The surface area and pore properties are deduced in inset Table 2 of Fig. 4 for clear understanding. From Table 2, the GNF material has a surface area of 8.5 m^2g^{-1} which is significantly increased to 155 m^2g^{-1}after N–doping. After α–MnO_2 is grown on N–GNF, the surface area of α–MnO_2/N–GNF is found to be 150 m^2g^{-1} whereas the surface area of α–MnO_2 nanorod is 25.5 m^2g^{-1}. The surface area of α–MnO_2/N–GNF is still much better than the original surface area. Similarly the pore volume and diameter of GNF also increased after N–doping. During the preparation process of N–doped carbon materials, nitrogen atoms substitute some carbon atoms that are located on the reactive edge, and ammonia also reacts with carbon to form hydrogen cyanide and hydrogen ($C + NH_3 = HCN + H_2$). This process consumed some carbon making the material more porous,

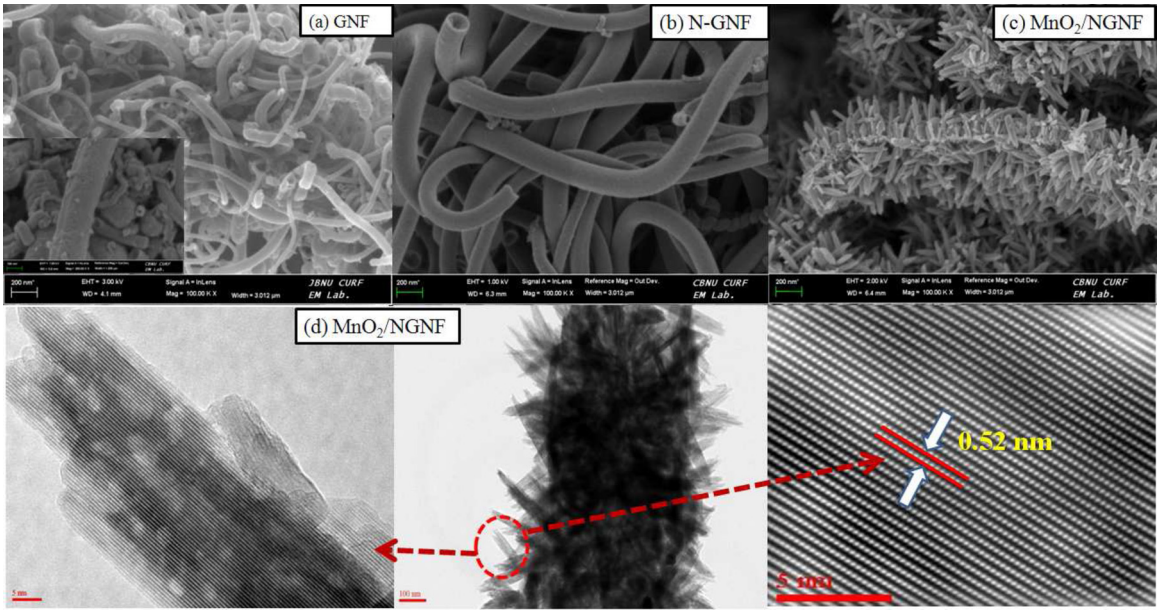

Fig. 3. SEM images of (a) GNF, (b) NGNF and (c) α–MnO_2/NGNF; and (d) HRTEM images of α–MnO_2/NGNF.

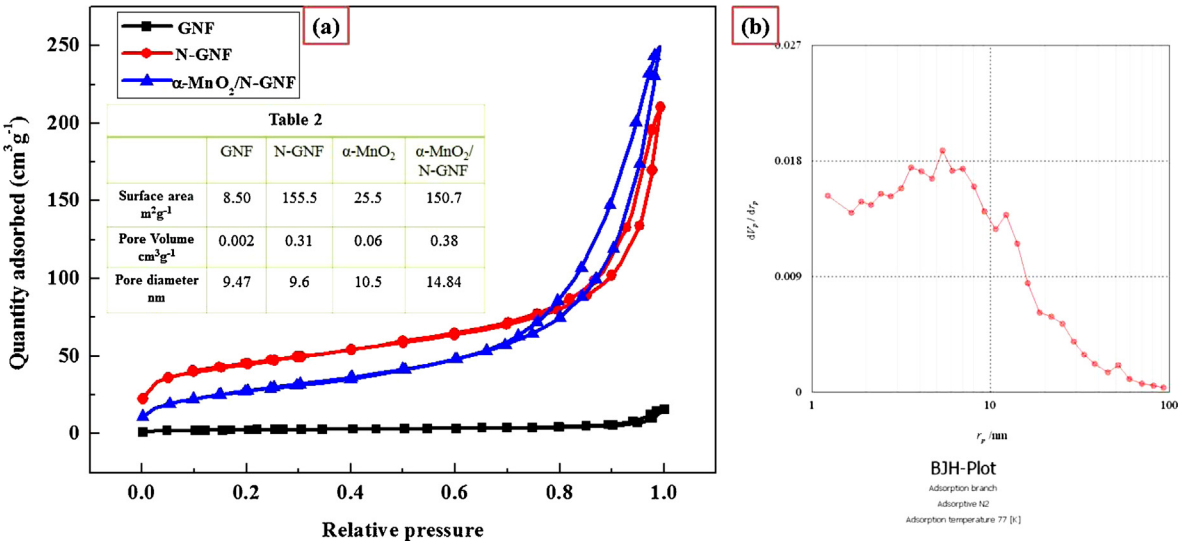

Fig. 4. (a) N_2 adsorption/ desorption isotherm of GNF, N-GNF and α-MnO_2/NGNF; (b) BJH plot of α-MnO_2/NGNF; (inset Table 2 BET surface area analysis of GNF, N-GNF, α-MnO_2 and α-MnO_2/NGNF).

resulting in the higher specific surface area and pore volume [24,25]. It can be noticed that the pore volume and diameter further increases for α–MnO_2/N–GNF. This shows that the α–MnO_2 grown on NGNF is also porous in nature. From the N_2 adsorption/ desorption isotherm based on the adsorption of N_2 gas on a material surface, it can be seen that N–GNF has mesoporous structure which is further improved with high N_2 uptake for α–MnO_2/N–GNF. These observations clearly explain the porous nature of as–prepared α–MnO_2/N–GNF with improved surface properties such as surface area and volume. The pore size distributions were calculated using the BJH (Barrett–Joyner–Halenda) plot from BET measurement. Fig. 4(b) shows the pore size distribution patterns of α–MnO_2/N–GNF from which the average pore size is calculated to be 5.35 nm.

3.2. Electrochemical properties

The performance of caterpillar shaped α–MnO_2/N–GNF catalyst for ORR/OER in Li–O_2 air cathode was evaluated in Swagelok™ type cells with 1 M LiTFSI (TEGDME) electrolyte and Li anode. The Li–O_2 cell performance was tested galvanostatically in a potential window of 2∼4.3 V. Fig. 5 shows the discharge/charge curves for Li–O_2 battery measured at 0.1 mA/cm^2. The first discharge starts from the open circuit potential of 3.2 V with a steady plateau at 2.8 V and attains a maximum discharge capacity of 2943 mAh/g. On charging a maximum of 99% capacity retention is achieved with a capacity of 2907 mAh/g and a potential gap of ΔV = 1.5 V. This discharge capacity is better than air cathode without any electro–catalyst [27] and with other α–MnO_2 based catalysts [7–10,15,23]. As the cycling number increases, the specific capacity dramatically increases, while the decrease in ΔV is observed. The second discharge capacity is 3066 mAh/g, and the third and fourth discharge capacities are recorded to be 3736 and 4706 mAh/g, respectively, as shown in Fig. 5(a). But it is seen that the specific capacity starts to dwindle after a steady increase in capacity for few cycles (1–4 cycles). The 5th and 6th discharge capacities are recorded to be 4450 and 3900 mAh/g, respectively. Even after 7 cycles (2300 mAh/g), the discharge capacity remains above 2000 mAh/g. The specific capacity with respect to cycle number is also shown in inset of Fig. 5. This charge–discharge characteristic is unusual for most bifunctional catalysts to show the gradual increase of the capacity with cycle number from the 1st cycle.

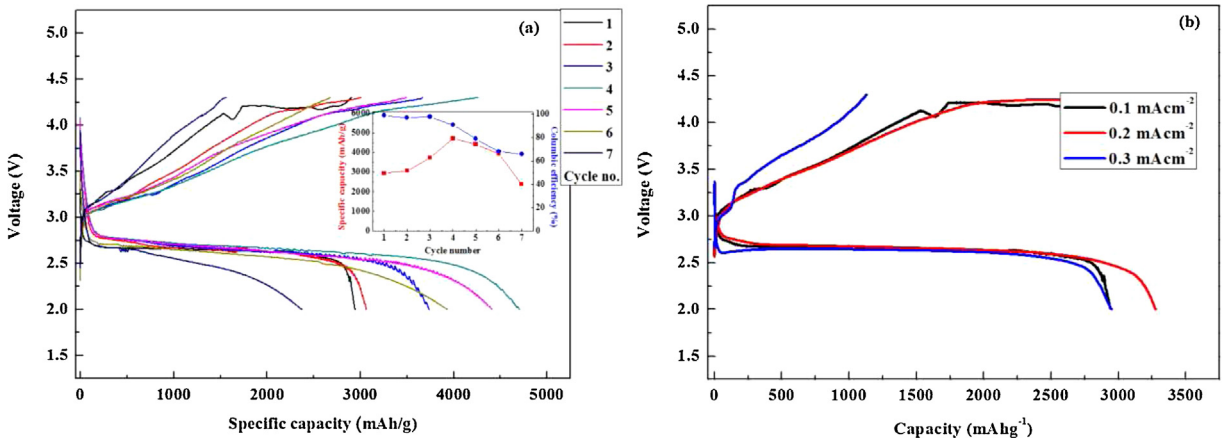

Fig. 5. (a) Charge–discharge curves of α-MnO_2/NGNF cathode at 0.1 mA/cm^2; inset Figure shows specific capacity and efficiency with respect to cycle number derived from (a); (b) First cycle capacities of α-MnO_2/NGNF cathode at 0.1, 0.2 and 0.3 mA/cm^2.

Similar observations have been previously reported for Li–O_2 batteries [15,28–30]. It has been explained that the discharge capacity behavior was because the ORR/OER activity of their catalysts promoted the cell reaction near the active sites of the catalyst resulting in the decrease in overpotential and the increase in cycle performance [28], which is discussed in detail in the later section. The α–MnO_2/N–GNF catalyst employed in our experiment also exhibit higher discharge voltage and lower charge voltage with higher discharge capacities than pure carbon based cell [15,28]. This indicates that our α–MnO_2/N–GNF catalyzed Li–O_2 battery is highly reversible during the discharge/charge processes. To attain the reliability of the data, the discharge–charge profiles were repeatedly measured for more than twice in this experiment.

In order to check the rate capability of our synthesized α–MnO_2/N–GNF catalysts, the first discharge capacities of the Li–O_2 battery were tested at higher current densities of 0.2 and 0.3 mA/cm^2 as well, and compared with that at 0.1 mA/cm^2. The cycle rate capabilities of the α–MnO_2/N–GNF catalyzed Li-O_2 battery are 2943 mAh/g and 3260 mAh/g for 0.2 and 0.3 mA/cm^2, respectively, as given in Fig. 5(b). Even with higher current densities we obtain better and almost similar specific capacity (∼3000 mAh/g). The overpotential observed for the higher current densities also remains to be 1 ± 0.2 V, which is comparable to (or better than) other MnO_2 based catalysts. Kim et al. [15] has compared the discharge capacities of cathode materials containing MnO_2 as the catalyst in Li–air batteries. According to Kim et al., their rGO/α–MnO_2 catalyst exhibited better performance at ≈0.3 mA/cm^2 than other MnO_2 based catalysts such as Pd/MnO_2 [7], α–MnO_2/Pd [8], α–MnO_2/CNT/CNF [31], and α–MnO_2 [9]. The comparison of catalytic properties of our synthesized α–MnO_2/CNF to the reported data shows that our α–MnO_2/N–GNF is one of the best performing bifunctional electrocatalyst, better than the other mentioned catalysts with high reversibility and rate capability. This presents that our synthesized α–MnO_2/N–GNF catalyst shows a highly stable catalytic activity even at higher electrochemical reaction kinetics.

In order to check the cyclability at a limited discharge capacity, we limited the depth of discharge at 500 mAh/g and observed the cycling properties of α–MnO_2/N–GNF catalyst for 50 cycles. It can be seen from Fig. 6(a) that there is a steady cycling property with no significant change in discharge potential but with a slight increase in the charge overpotential, while maintaining charge/discharge capacities for 50 cycles with 100% efficiency (inset Fig. 6(a)). The charge and discharge potentials of α–MnO_2 were also measured at a limited discharge capacity of 500 mAh/g and depicted in Fig. 6(b) as a function of cycle number together with those of α–MnO_2/N–GNF extracted from Fig. 6(b) for comparison. The potential gap is maintained between 1∼1.5 V whereas the discharge potential almost remains constant. The discharge potential of α–MnO_2/N–GNF is lesser than the α–MnO_2 only cells and is steadily maintained without any increase in potential for 50 cycles. Meanwhile, the charge potential of α–MnO_2/N–GNF is far lesser than α–MnO_2 only cells. Even though a slight increase in charge potential is observed at about 20 cycles, the potential is maintained up to 50 cycles as shown in the Fig. 6(b). For the α–MnO_2 only catalyst, however, the voltage gap is initially higher than that of α–MnO_2/NGNF catalyst and starts to increase after 20 cycles. But it rapidly falls out of range from the cycle number about 40 cycles. This identifies that our prepared α–MnO_2/N–GNF nanostructure exhibits a better catalytic activities for both ORR and OER in Li–O_2 battery. It has been reported that Li–O_2 batteries requires very high potential for OER on charging in cathode due to the formation of solid discharge products during ORR on discharge. The increase of overpotential with respect to cycle number causes the degradation of cathode performance and the decomposition of electrolytes, resulting in low round trip efficiency of the battery. This is one of the main challenges being faced by the Li–O_2 battery technology. In our case, however, we observed a decrease in overpotential in every cycle for the first few cycles (complete cycling) as seen in Fig. 5(a). Even after the first 5 cycles, there was not much observable increase in overpotential. When we examined the cyclability at a limited discharge capacity, the discharge and charge potential difference, ΔV, of α–MnO_2/N–GNF catalyst was much smaller and stable than that of only α–MnO_2 catalyst maintaining 100% efficiency of charge/discharge capacities for 50 cycles as shown in Fig. 6(a). It was clearly shown from the experiments that the main advantage of our synthesized α–MnO_2/N–GNF bifunctional electrocatalyst is to decrease the potential gap and exhibits a better catalytic activity for both ORR and OER in Li–O_2 battery.

The reason why the better cycling profiles were attained from our synthesized catalyst might be due to the additional carbon support rendered by N–GNF to α–MnO_2 catalyst. It is well known that α–MnO_2 catalysts exhibit better ORR characteristics [9–12]. The increased electrocatalytic activity of the α–MnO_2 is mainly because of the large 2 × 2 tunnel structures which favor the accommodation of Li_2O_2. According to the mechanism reported by previous literatures [10,32–34], Li_2O_2 can be incorporated within the MnO_2 tunnels with the O_2 ions located at the tunnel centres and the Li^+ ions coordinated between these central O_2 ions forming the walls of the tunnels. In addition, α–MnO_2 contains more defects and OH^- groups which are beneficial to surface adsorption

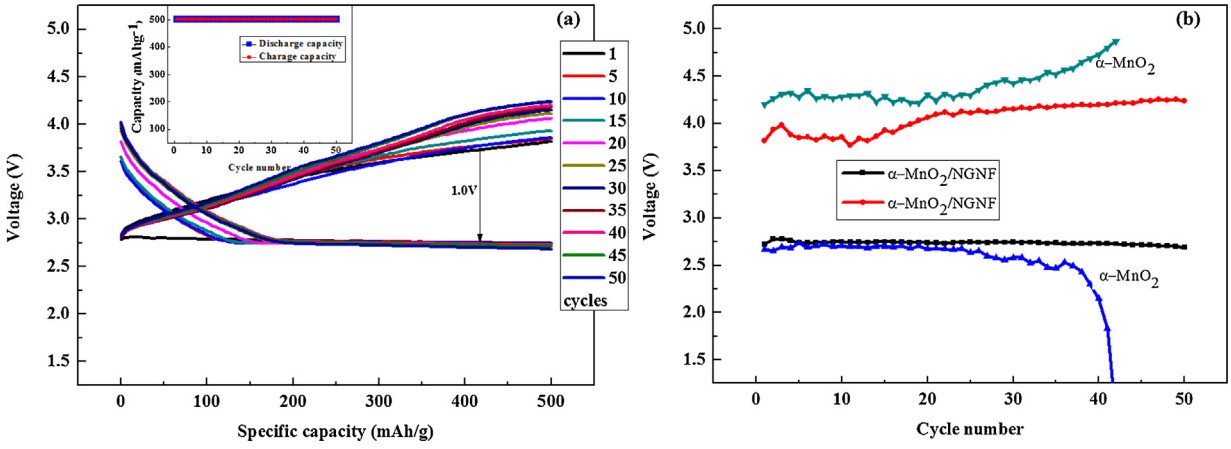

Fig. 6. (a) (and inset) Cyclability of α-MnO_2/NGNF cathode up to 50 cycles; (b) Discharge and charge potentials of α-MnO_2 and α-MnO_2/NGNF with respect to cycle number.

of O_2 and dissociation of O–O bonds. Also α phase of MnO_2 has an average Mn–O bond length of 1.98 °A. This length is weaker than other phases of MnO_2 structures and hence α–MnO_2 has less reaction barriers which facilitate the reaction kinetics [35,36]. Meanwhile, GNF helps to connect the α–MnO_2 nanorods to provide high surface area and improves electron transfer by acting as a conductive medium. GNF affords high electron conductivity due to their high degree of graphitization and provides fast ion transport because of their mesoporous network [22]. In addition, GNF exhibits excellent electrocatalytic property than disordered carbons due to its superior structural and electrochemical characteristics which includes high specific surface area and uniform porosity [19–21]. Thus it is considered that the synergic effect of caterpillar structured α–MnO_2/N–GNF bifunctional catalyst enhances the overall efficiency of the Li–O_2 battery.

It has been also reported that the N doping in GNF increases both the reaction surface area in the electrocatalytic reaction and the ORR activity of the material [23,24]. According to the BET data shown in Table 2, the surface area of N–GNF was highly increased on N doping. The surface area of α–MnO_2/N–GNF hybrid was more than 10 and 4 times higher than the original GNF and α–MnO_2, respectively. This shows that the widened surface area facilitates the cell reaction by providing a large surface area for the formation of Li_2O_2. In addition to the increased surface area, the material showed higher porosity (Fig. 4) with increase in mesopore volume on N doping. This increase in pore features helps to contain more Li_2O_2 during the reaction process. In addition, porous surface facilitates the O_2 and electrolyte diffusion resulting in the improved overall reaction mechanism. Regarding the ORR activity, the incorporation of nitrogen increases the electrocatalytic activity by introducing structural defects. The fact that N–doped carbons exhibit better electrocatalytic activity has been well established [23,24,37–42]. The doped nitrogen with lone electron pair provides negative charges and increases the interaction with the adjacent carbon atoms with high positive charge density which results in the enhanced ORR activity [23,24].

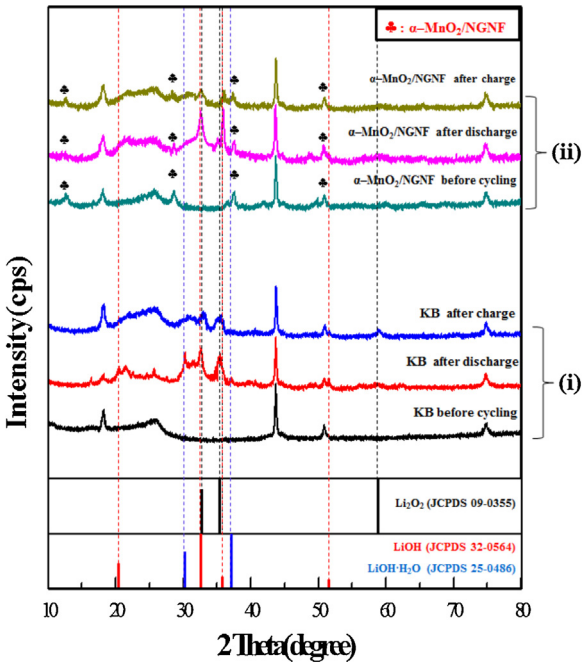

Fig. 7. XRD spectra of air cathodes (i) without any catalyst and (ii) with our synthesized α–MnO_2/NGNF catalyst measured before and after discharge/charge.

Another important reason for the better Li–O_2 battery performance is the proper decomposition of discharge products on the electrode surface. Many efforts have been focused on the development of electrocatalysts active for Li_2O_2 formation and decomposition reactions, but the most of the catalysts also catalyzed the formation/decomposition of lithium carbonates on the electrode surface as well as decomposition of electrolytes. However, our synthesized α–MnO_2/NGNF bifunctional catalyst seems to actively participate only in the formation and decomposition reaction of Li_2O_2. The columbic efficiency (99%) between discharge and charge capacities at the 1st cycle (in the inset of Fig. 5(a)) shows the proper formation and decomposition of reaction products.

In order to confirm the reversible formation of Li_2O_2 during discharge–charge cycling, post analysis of the electrode was performed. For the analysis, the surface of air cathode before and after discharge/charge processes were examined for the formation and decomposition of Li_2O_2 using XRD and SEM techniques. Fig. 7 shows the XRD spectra which were measured before and after discharge/charge during the first cycle for α–MnO_2/NGNF catalyzed air cathodes. For comparison same set of XRD spectra for KB electrode without any catalyst was also measured. The carbon (for active material KB at 2θ = 23°, 44°), TAB (for binder at 2θ = 17°), and Ni (for current collector at 2θ = 43.5°, 47.6° and 51°) peaks are observed from all the XRD spectra. The traces of LiOH observed in the XRD spectra after discharge process might be due to the reaction of Li_2O_2 with the structural water content in MnO_2 [43]. For the KB air cathode (i) without any catalyst, the XRD spectrum before discharge cycling shows characteristic peaks for KB at 2θ = 23°, 44°. After the first discharge, as expected, the XRD peaks shows the formation of Li_2O_2 at 2θ = 32°, 35° and 58° as discharge product. After the first charge, the Li_2O_2 peaks almost remain on the electrode surface as it was observed after the discharge process. The appearance of Li_2O_2 peaks even after charging process indicates the poor decomposition of Li_2O_2 on the surface of KB electrode. In the case of our synthesized α–MnO_2/N–GNF catalyzed air cathode (ii), α–MnO_2 and carbon (GNF) peaks are clearly observed in the XRD spectrum before discharge. After discharge, the XRD peaks clearly shows the formation of Li_2O_2 at 2θ = 32°, 35° and 58° with a trace of LiOH at 2θ = 32.4° and 35.6°. After charging the Li_2O_2 peaks have almost disappeared from the XRD spectrum as compared to that of the KB cathode, indicating the decomposition of Li_2O_2. This confirms that our synthesized α-MnO_2/N–GNF catalyzed air cathode helps in the reversible formation of Li_2O_2.

Fig. 8 shows the SEM images which were taken before and after discharge/charge during the first cycle for air cathodes (i) without any catalyst and (ii) with our synthesized α–MnO_2/N–GNF catalyst. From the SEM images taken before discharge, it can be seen that both the air cathodes (i) without catalyst and (iii) with our synthesized α–MnO_2/N–GNF catalyst shows a smooth surface without much differences. After the first discharge, the KB air cathode without any catalyst shows the formation of agglomerations all over the cathode surface. Also, the air cathode with our synthesized α–MnO_2/N–GNF catalyst shows the formation of agglomerations on the cathode surface at a different configuration. This formation of agglomerations after discharge processes clearly shows the formation of Li_2O_2 as shown in Fig. 8. After charging, however, the air cathode (i) without any catalyst shows almost similar agglomeration to remain, as observed in the XRD, indicating only poor decomposition of Li_2O_2. On the other hand, the air cathode with our synthesized α-MnO_2/N–GNF catalyst shows almost similar cathode surface to that of the original one before discharge/charge cycle indicating the decomposition of Li_2O_2. This SEM data persistent with the XRD data explains that our synthesized α–MnO_2/N–GNF catalyst is an efficient ORR/OER

catalyst for the reversible formation of Li_2O_2. Nonetheless, the traces of remaining Li_2O_2 in both XRD and SEM attest to the fade in capacity after first few cycles.

The increase in capacity in the first few subsequent cycles might be due to the gradual activation mechanism of the electrocatalyst which is favorable for the improvement of electrochemical kinetics [28]. Similar behavior in the discharge–charge profiles of Li air battery has been reported in previous literatures [28–30] etc. The catalytic activity of the electrocatalyst promotes the formation of discharge products near the active sites of catalyst followed by the formation on carbon surface. Our synthesized α–MnO_2/N–GNF actively promoted the ORR and OER in the active sites of the air cathode and during the first few cycles the carbon cathode surface is also activated gradually. From Figs. 7 and 8, it can be seen that no intermediate/insoluble products like Li_2CO_3 are formed during the first discharging. Generally, formation of such intermediate products will increase the OER potential on charging and degrade the cell capacity upon cycling. In this case, however, the α–MnO_2/N–GNF catalyst activates the ORR/OER mechanism and promotes the reversible formation of only Li_2O_2. Thus, while α–MnO_2/N–GNF maintains a steady cycling efficiency throughout, the activation of carbon surface in every cycle might be the reasons for the increasing capacity, high discharge voltage and low charge voltage observed during the first four cycles in our α–MnO_2/N–GNF catalyzed air cell. Another reason for the subsequent increase and decrease in the capacity during the first few cycles might be attributed to the stability of our α–MnO_2/N–GNF catalyst which does not modify the cathode surface upon discharge–charge cycling. However, it can be seen that the specific capacity started to fade after a steady increase in capacity for four cycles (1–4 cycles). During the reversible formation of Li_2O_2 in the charge discharge process after few cycles, there are possibilities for the carbon in the cathode surface to react with the discharge product Li_2O_2 and form irreversible side products. So after the first few cycles, the capacity starts to decrease since these side products could form a non–conductive film on the cathode surface terminating any further reactions. Another possible reason for the fade in capacity after first four cycles might be that, sometimes, the Li_2O_2 might form deep inside the pores on the electrode surface and do not reverse back on charging, resulting in the attenuation of cell cycling. It is assumed that the Li_2O_2 might be initially formed in a uniform size all over the catalyst surface. In larger pores the Li_2O_2 may be readily removed during charge because of more flat and wide surface. But deep inside the pores, however, the Li_2O_2 formed during discharge are easy to agglomerate together to form larger clusters or a film that covers or blocks the active sites of catalyst surface. This degrades the catalyst activity which results in the gradual decrease of the battery performance. In order to identify this explanation, we calculated the coulomb's efficiency for the capacities which is shown in Fig. 5(a) inset. According to the inset in Fig. 5(a), up to 4 cycles when the cell shows increase of discharge capacity, the efficiency is maintained more than 90%. But the Figure presents a decrease of efficiency after cycle number 4 which supports that the decrease of discharge capacity is due to the remaining Li_2O_2 after charging process.

Apart from active electrocatalyst, selection of electrolyte is also essential to determine the nature of discharge products and rechargability of the battery. Tetra ethylene glycol dimethyl ether (TEGME) used in this study is a popularly used electrolyte for Li–O_2 batteries. Unlike other carbonate based electrolytes, Li_2O_2 was found to be the main discharge product when glyme–based electrolytes are employed [44–47]. Although ethers are relatively stable electrolytes against nucleophilic attack, the long–term stability is still lacking as they are prone to auto-oxidation under oxygenated radicals to be converted into unstable peroxide species [45,46]. This might be the reason why the fade in capacity is observed after first few cycles even after the impressive behavior of α–MnO_2/N–GNF bifunctional catalysts. In order to improve the stability of the Li–O_2 battery with α–MnO_2/N–GNF catalysts and obtain over all better cyclability, further detailed studies based on electrolytes are underway.

It is very clear that the combined effect of α–MnO_2 and N–GNF results in the increased reversibility of the battery. As explained in the previous sections, the α–MnO_2 in the α–MnO_2/N–GNF exhibits desirable catalytic activity for both ORR and OER processes. The N–GNF in the α–MnO_2/N–GNF helps to improve the conductivity, and provides high surface area and pore properties. Other factors like porosity of the cathode, oxygen pressure and suitable electrolyte

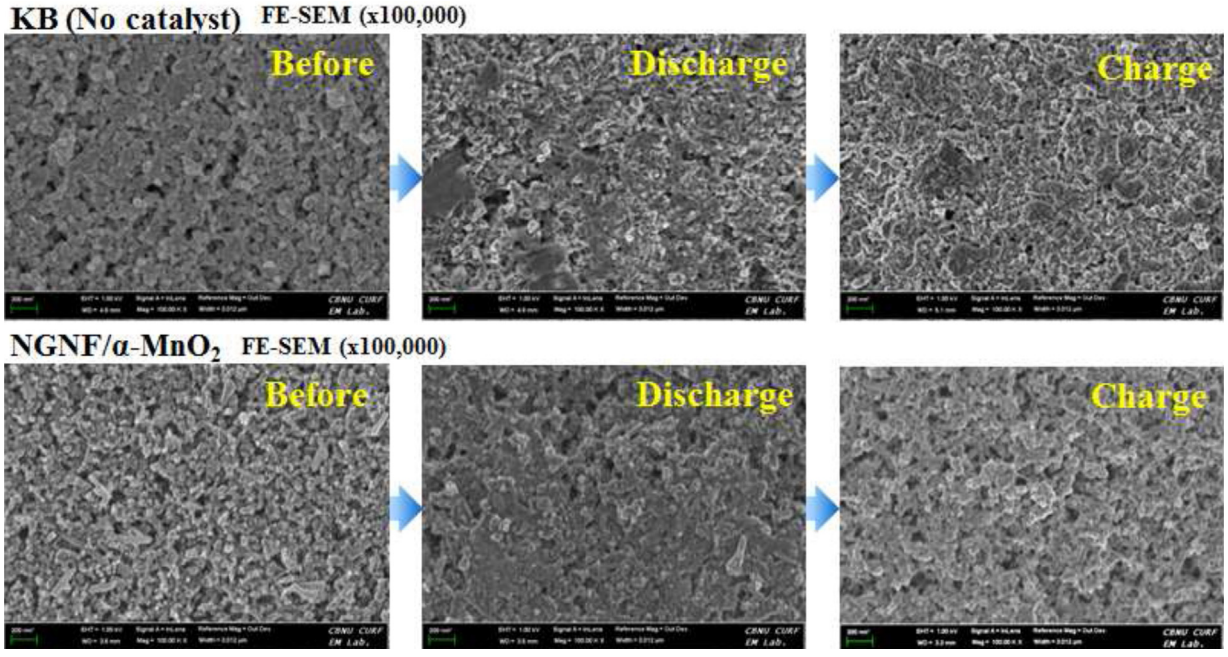

Fig. 8. SEM images of air cathodes (i) without any catalyst and (ii) with our synthesized α–MnO_2/NGNF catalyst measured before and after discharge/charge.

can also influence the cell efficiency. The electrocatalytic activity is mainly determined by the reversible adsorption/desorption of reactants/products. The α–MnO_2/N–GNF nanostructures is considered to contributes its maximum for ORR and OER activity resulting in almost complete reversibility on charge and discharge capacity upon cycling.

4. Conclusions

We have successfully developed α–MnO_2/NGNF nanomaterials as bifunctional electrocatalyst for Li–O_2 air cathodes. The superior ORR and OER activity of α–MnO_2 in the air cathode significantly improved the reversible capacity of Li–O_2 batteries. The highly conductive nature of GNF connects the α–MnO_2 nanorods and N doping in NGNF increased the surface properties of the electrode. The collective effects of developed caterpillar shaped α–MnO_2/NGNF resulted in the better performance of Li–O_2 cell with high capacity and reversibility of the battery. The main advantage of our synthesized α–MnO_2/NGNF bifunctional electrocatalyst is the low potential gap. In addition to the high reversibility, α–MnO_2/NGNF catalyzed air cathode exhibited very good rate capability with discharge capacity as high as ∼3000 mAh/g for 0.1, 0.2 and 0.3 mA/cm^2. Also α–MnO_2/NGNF catalyzed air cathode was very stable up to 50 cycles with high efficiency.

Acknowledgment

This work was supported by the Human Resources Development program (No.20114030200060) of the Korea Institute of Energy Technology Evaluation and Planning (KETEP) grant funded by the Korea government Ministry of Trade, Industry and Energy. This work is also supported by Basic Science Research Program through the National Research Foundation (NRF) funded by the Ministry of Education (No. 2013R1A1A2012656).

References

[1] G. Girishkumar, B. McCloskey, A.C. Luntz, S. Swanson, W. Wilcke, Journal of Physical Chemistry Letters 1 (2010) 2193–2203.
[2] A. Zahoor, M. Christy, Y. Hwang, K.S. Nahm, Journal of Electrochemical Science and Technology 3 (1) (2012) 14–23.
[3] H.G. Jung, J. Hassoun, J.B. Park, Y.K. Sun, B. Scrosati, Nature Chemistry 4 (2012) 579–585.
[4] B.D. McCloskey, A. Speidel, R. Scheffler, D.C. Miller, V. Viswanathan, J.S. Hummelshøj, J.K. Nørskov, A.C. Luntz, Journal of Physical Chemistry Letters 3 (8) (2012) 997–1001.
[5] Z. L. Wang, D. Xu, J. J. Xu, X. B. Zhang, Chemical Society Reviews, (2013) Advance Article DOI: 10.1039/c3cs60248f.
[6] Z.Y. Lu, Z. Xu, H.A. Gasteiger, S. Chen, K. Hamad-Schifferli, Y.J. Shao-Horn, Journal of the American Chemical Society 132 (2010) 12170–12171.
[7] A.K. Thapa, K. Saimen, T. Ishihara, Electrochemical Solid-State Letters 13 (2010) A165–A167.
[8] A.K. Thapa, T. Ishihara, Journal of Power Sources 196 (2011) 7016–7020.
[9] A. Debart, J. Bao, G. Armstrong, P.G. Bruce, Journal of Power Sources 174 (2007) 1177–1182.
[10] A. Debart, A.J. Paterson, J. Bao, P.G. Bruce, *2008*, Angewandte Chemie International Edition 47 (*2008*) 4521–4524.
[11] K. Song, J. Jung, Y. Heo, Y.C. Lee, K. Cho, Y.M. Kang, Physical Chemistry Chemical Physics 15 (2013) 20075–20079.
[12] A. Zahoor, H.S. Jang, J.S. Jeong, M. Christy, Y. Hwang, K.S. Nahm, RSC Advances 4 (2014) 8973–8977.
[13] X. Hu, F. Cheng, X. Han, T. Zhang, J. Chen, Small, (2014) DOI: 10.1002/smll.201401790.
[14] J. Li, N. Wang, Y. Zhao, Y. Ding, L. Guan, Electrochemistry Communications 13 (2011) 698–700.
[15] Y. Yu, B. Zhang, Y.B. He, Z.D. Huang, S.W. Oh, J.K. Kim, Journal of Materials Chemistry A 1 (2013) 1163–1170.
[16] S. Khilari, S. Pandit, M.M. Ghangrekar, D. Das, D. Pradhan, RSC Advances 3 (2013) 7902–7911.
[17] H. Chen, S. Zhou, M. Chen, L. Wu, Journal of Materials Chemistry 22 (2012) 25207–25216.
[18] H.W. Park, D.U. Lee, L.F. Nazar, Z. Chen, Journal of The Electrochemical Society 160 (2) (2013) A344–A350.
[19] C.A. Bessel, K. Laubernds, N.M. Rodriguez, R.T.K. Baker, Journal of Physical Chemistry B 105 (2001) 1115–1118.
[20] L. Gan, H. Du, B. Li, F. Kang, Chemical Communications 47 (2011) 3900–3902.
[21] Z. Tai, X. Yan, J. Lang, Q. Xue, Journal of Power Sources 199 (2012) 373–378.
[22] R.R. Mitchell, B.M. Gallant, C.V. Thompson, Y.S. Horn, Energy and Environmental Science 4 (2011) 2952–2958.
[23] Y. Li, J. Wang, X. Li, J. Liu, D. Geng, J. Yang, R. Li, X. Sun, Electrochemistry Communications 13 (7) (2011) 668–672.
[24] A. Zahoor, M. Christy, Y. Hwang, Y.R. Lim, P. Kim, K.S. Nahm, Applied catalysis B 147 (2014) 633–641.
[25] J. Yin, Y. Qiu, J. Yu, ECS Solid State Letters 2 (5) (2013) M37–M39.
[26] A. Zahoor, H.S. Jang, J.S. Jeong, M. Christy, Y. Hwang, P. Kim, K.S. Nahm, Science of Advanced Materials 6 (2014) 2712–2723.
[27] A.A. Franco, K.H. Xue, ECS Journal of Solid State Science and Technology 2 (10) (2013) M3084–M3100.
[28] K. Zhang, L. Zhang, X. Chen, X. He, X. Wang, S. Dong, P. Han, C. Zhang, S. Wang, L. Gu, G. Cui, Journal of Physical Chemistry C 117 (2013) 858–865.
[29] H. Cheng, K. Scott, Journal of Power Sources 195 (2010) 1370–1374.
[30] D. Zhu, L. Zhang, M. Song, X. Wang, Y. Chen, Chemical communications 49 (2013) 9573–9575.
[31] G.Q. Zhang, J.P. Zheng, R. Liang, C. Zhang, B. Wang, M. Au, M. Hendrickson, E.J. Plichta, Journal of the Electrochemical Society 158 (2011) A822–A827.
[32] C.S. Johnson, D.W. Dees, M.F. Mansuetto, M.M. Thackeray, D.R. Vissers, D. Argyriou, C.K. Loong, L. Christensen, Journal of Power Sources 68 (1997) 570–577.
[33] J.E. Post, Proc. Natl. Acad. Sci. U. S. A. 96 (1999) 3447–3454.
[34] W. Xiao, D. Wang, X.W. Lou, Journal of Physical Chemistry C 114 (2010) 1694–1700.
[35] F. Cheng, Y. Su, J. Liang, Z. Tao, J. Chen, Chemistry of Materials 22 (2010) 898–905.
[36] S.H. Liang, F. Teng, G. Bulgan, R.L. Zong, Y.F. Zhu, Journal of Physical Chemistry C 112 (2008) 5307–5315.
[37] K. Gong, F. Du, Z. Xia, M. Durstock, L. Dai, Science 323 (2009) 760–764.
[38] E.Y.F. Tang, B.L. Allen, D.R. Kauffman, A. Star, Journal of the American Chemical Society 131 (2009) 13200–13201.
[39] F.L. Qu, Y. Liu, J.B. Baek, L. Dai, ACS Nano 4 (2010) 1321–1326.
[40] G.S. Chen, J.Y. Bi, Y. Zhao, L.J. Yang, C. Zhang, Y.W. Ma, Q. Wu, X.Z. Wang, Z. Hu, Advanced Materials 24 (2012) 5593–5597.
[41] H.E. Yoo, J. Nakamura, H. Zhou, Energy and Environmental Science 5 (2012) 6928–6932.
[42] P. Kichambre, J. Kumar, S. Rodrigues, B. Kumar, Journal of Power Sources 196 (6) (2011) 3310–3316.
[43] B. Sun, P. Munroe, G. Wang, Scientific Reports 3 (2013) 2247.
[44] S.A. Freunberger, Y. Chen, Z. Peng, J.M. Griffin, L.J. Hardwick, F. Barde, P. Novak, P.G. Bruce, Journal of the American Chemical Society 133 (2011) 8040–8047.
[45] B.D.M. cCloskey, D.S. Bethune, R.M. Shelby, G. Girishkumar, C. Luntz, Journal of Physical Chemistry Letters 2 (2011) 1161–1166.
[46] S.A. Freunberger, Y. Chen, N.E. Drewett, L.J. Hardwick, F. Bard, P.G. Bruce, Angewandte Chemie International Edition 50 (2011) 8609–8613.
[47] M. Balaish, A. Kraytsberg, Y. Eli, Physical Chemistry Chemical Physics 16 (2014) 2801–2822.